CORROSION INHIBITION AND ADSORPTION BEHAVIOR OF NEW SCHIFF BASE SURFACTANT ON STEEL IN ACIDIC ENVIRONMENT: EXPERIMENTAL AND THEORETICAL STUDIES

S.A. SOLIMAN[(a)], M.S. METWALLY[(a)], S.R. SELIM[(a)], M.K. AWAD [(b)] , MOHAMED.A. ABBAS[(c)], AND M.A. BEDAIR[(a,*)]

(a) Chemistry Department, Faculty of Science, Al-azhar University, Cairo, Egypt.
(b) Chemistry Department, Theoretical Applied Chemistry Unit (TACU), Faculty of Science, Tanta University, Egypt.
(c) Egyptian Petroleum Research Institute (EPRI), Cairo, Egypt.

(*)Corresponding author: m_bedier@yahoo.com , Mobile +201014134321

Abstract

Synthesis, adsorption and corrosion inhibiting effect of new Schiff base surfactant named 4-Hydroxy -3-(3-phenyl-allylideneamino)-benzene sulphonic acid2-[2-(2-{2-[2-(2-hydroxy-ethoxy)-ethoxy]-ethoxy}-ethoxy)-ethoxy]-ethyle ether (abbreviated as PAAB) on mild steel in 1.0 M HCl was investigated using weight loss and potentiodynamic polarization techniques. The results revealed that this compound inhibited the corrosion reaction in HCl environment. The results indicated that this inhibitor was adsorbed on the metal/solution interface. A theoretical study of the adsorption behavior of this compound was carried out in the framework of the semiempirical (SE) and molecular dynamics (MD).

Keywords: Weight loss, Potentiodynamic polarization, Adsorption isotherm, Schiff base surfactant, Quantum chemical studies.

Introduction

Acid solutions are often used in drilling operations in oil and gas exploration, as well as for cleaning, descaling and pickling of steel structures; processes which are normally accompanied by considerable dissolution of the metal. A useful method to protect metals and alloys deployed in service in such aggressive environments against corrosion is addition of species to the solution in contact with surface in order to inhibit the corrosion reaction and reduce the corrosion rate. Most of acid corrosion inhibitors are organic compounds containing electronegative atoms (such as, N, S, P and O), unsaturated bonds (such as, double or triple bonds), and plane conjugated systems including all kinds of aromatic cycles [1–11]. Some research works revealed that the inhibition efficiency of Schiff bases is much greater than that of corresponding amines and aldehydes due to the presence of a –CH=N- group in the molecules [12]. The surfactant inhibitors have many advantages such as high inhibition efficiency, low price, low toxicity and easy production [13–18]. The aim of the present work is to investigate the corrosion inhibition and the inhibition mechanism of the prepared nonionic surfactant for steel in 1.0 M hydrochloric acid.

Materials and Experimental Methods

Materials

Tests were performed on steel of the composition: (0.11% C, 0.45% Mn, 0.04% P, 0.05% S, 0.25% Si, and the remained is Fe).

Inhibitor

The Schiff base surfactant was prepared via two steps; the first one is Schiff base reaction between 3-amino-4-hydroxybenzenesulphonic acid and cinnmaldehyde in the molar ratio of 1:1 each reactant was dissolved in 50 ml ethyl alcohol and refluxed for 1 hour then the reaction mixture was left to cool and filtered. The product was washed and dried to give red crystals of the produced Schiff base. The second step is esterfication reaction with poly ethylene glycol (M.wt =300) with 1:1 molar ratio, xylene as solvent and p-toluene sulphonic acid as dehydrating agent refluxed for 6 hours. The product washed and dried to give faint red crystal of nonionic surfactant (Scheme 1).

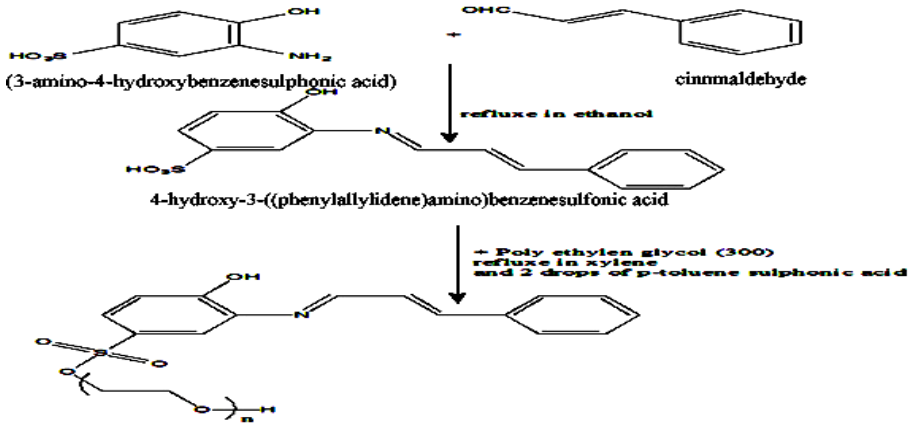

Scheme 1. Synthetic route of the studied Schiff base nonionic surfactant.

Solutions

The aggressive solution, 1.0 M HCl, were prepared by dilution of analytical grade 37% HCl with distilled water. The concentrations of the prepared surfactant used were: $1X10^{-4}$, $3X10^{-4}$, $5X10^{-4}$, $7X10^{-4}$ and $9X10^{-4}$ M. All solutions were prepared using distilled water.

Weight loss measurements

The experiments were carried out using steel specimens. The steel sheets of 6.0 × 2.5 × 0.3 cm with an exposed total area 35.1 cm^2 were used for weight loss

measurements. They were abraded with different grade of emery paper washed with distilled water, and dried in acetone and warm air. The precleaned and weighed coupons were suspended in beakers containing the test solutions using glass hooks and rods. Tests were conducted under total immersion conditions in 100 ml of the aerated test solutions. To determine weight loss with respect to time, test coupons were retrieved at 24 h intervals progressively for 96 h, scrubbed with a bristle brush, washed, dried and reweighed. The weight loss was taken as the difference between the initial and final weights of the coupons.

Electrochemical measurements

Electrochemical experiments were carried out using a Voltalab 40 Potentiostat PGZ 301 in a conventional electrolytic cell with three-electrodes arrangement: saturated calomel reference electrode (SCE), platinum rod as a counter electrode and the working electrode (WE) had the form of rod from steel. Prior to each experiment, the specimen was treated as in weight loss measurements. The electrode potential was allowed to stabilize for 30 min before starting the measurements. The exposed electrode area to the corrosive solution is 1 cm^2. All experiments were conducted at 25° C. Potentiodynamic polarization curves were obtained by changing the electrode potential automatically (from -1000 to -200 mV vs. SCE) at open circuit potential with a scan rate of 2 mV s^{-1}.

Quantum chemical calculations

Quantum chemical calculations were performed for the inhibitor. This surfactant molecule was completely optimized with PM6 semiempirical method. It was drawn using Gauss View, 5.0 implemented in Gaussian 09 package [19]. The corresponding geometries were optimized without any geometry constraints for full geometry optimization. Frequency calculations were executed simultaneous and no imaginary frequencies were found indicating a minimal energy structure. According to Koopman's theorem [20], the E_{HOMO} and E_{LUMO} of the inhibitor molecule are related to the ionization potential, I, and the electron affinity, A, respectively, by the following relations:

$$I = - E_{HOMO} \qquad A = - E_{LUMO} \tag{1}$$

Absolute electro negativity, X, and absolute hardness, η, of the inhibitor molecule are given by [21]:

$$X = \frac{(I+A)}{2} \qquad \eta = \frac{(I-A)}{2} \tag{2}$$

The obtained values of "X" and "η" were used to calculate the fraction of electron transferred, ΔN, from the inhibitor to metallic surface as follow [22]:

$$\Delta N = \frac{X\,fe - X\,inh}{2(\eta\,fe + \eta\,inh)} \qquad (3)$$

Molecular dynamic simulation

Molecular simulation studies were performed using Materials studio 4.3 software from Accelrys Inc. [23] which has been used to build surfactant molecule and Fe (1 1 1) surface (as steel) using the sketching tools in Materials Visualizer. COMPASS (Condensed Phase Optimized Molecular Potentials for Atomistic Simulation Studies) [24] is the first ab initio force field that enables accurate and simultaneous prediction of chemical properties (structural, conformational, vibrational, etc.) and condensed-phase properties (equation of state, cohesive energies, etc.) for a broad range of chemical systems. The first step in this computational study is the preparation of a model of molecules which will adsorb on the surface with optimized geometry (i.e. energy minimized). The MD simulation of the interaction between the surfactant molecule and the Fe surface (1 1 1) was carried out in a simulation box (22.90 ×57.26 ×26.68 A°) with periodic boundary conditions to model a representative part of an interface devoid of any arbitrary boundary effects. The box consists of a Fe slab and a vacuum layer of 15.00 Å heights. The interaction energy $E_{Fe\text{-}inhibitor}$ of the steel surface with the inhibitor was calculated according to the following equation:

$$E_{Fe\text{-}inhibitor} = E_{complex} - (E_{Fe} + E_{inhibitor}) \qquad (4)$$

where $E_{complex}$ being the total energy of Fe crystal together with the adsorbed inhibitor molecule. E_{Fe} and $E_{inhibitor}$ being the total energy of Fe crystal and free inhibitor molecules, respectively.

The binding energy was the negative sign value of interaction energy,

$$E_{binding} = - E_{Fe\text{-}inhibitor} \qquad (5)$$

Results and Discussion

Confirmation the chemical structure of the synthesized inhibitor

The chemical structure of the prepared surfactant was confirmed by the FTIR, NMR and Mass spectra as well as (C, H, N, S) analysis and are shown in Figs. (1-3) and Tables (1, 2).

FTIR spectrum

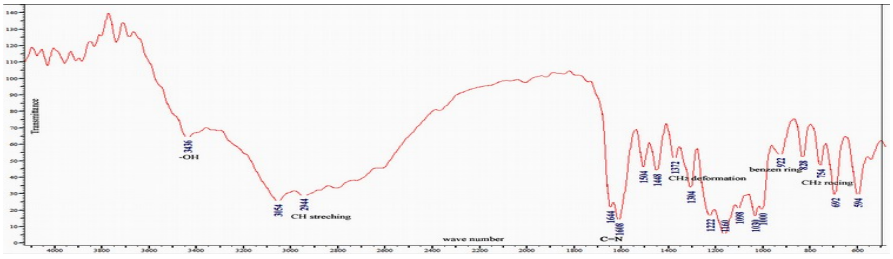

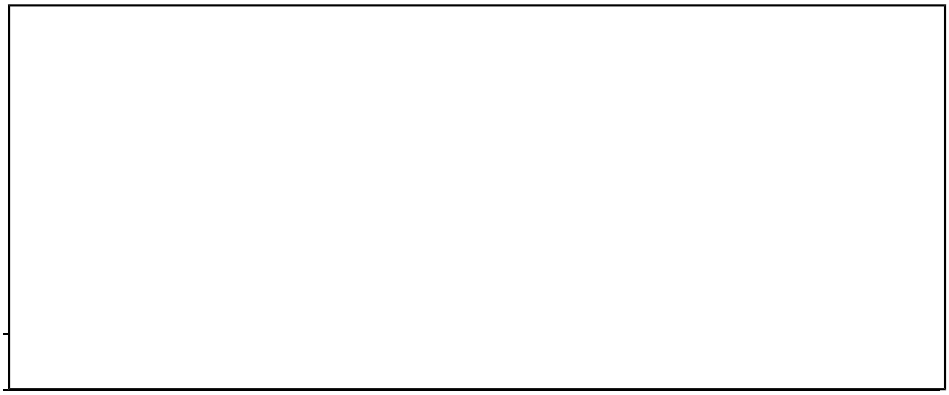

$(CH_2)_n$– rock.	754	(C=C) aromatic ring stretching	1504
(S-O,S=O) stretching	1030, 1160	(C=N)	1608
(CH_2) deformation	1372	Symmetric and symmetric stretching (CH)	2944
C,%H,%N,%S,			
%Found Symmetric	1448	Phenolic OH group	3436
bending (CH_2)			

56.034.723.395.76Expected 55.566.392.405.49

Weight Loss Measurements

Influence of inhibitor concentration on the corrosion rate

The corrosion rate of steel in the absence and presence of different concentrations of PAAB at 30ºC was studied using weight loss technique. Table 3 shows the calculated values of corrosion rate ($mg.cm^{-2}.h^{-1}$), inhibition efficiency (η_w) and the degree of surface coverage(Θ) for steel in 1.0 M HCl in the absence and presence of PAAB, which indicated its ability to inhibit the corrosion of steel in 1.0 M HCl solutions, where the corrosion rate depends on the concentration. As the concentration increases, the inhibition efficiency increases. The results also indicated that the corrosion rate increased with increasing exposure time and that PAAB actually retarded steel corrosion at all concentrations in 1.0 M HCl as shown in Fig. 4. The relation between η_w of steel and logarithm of the inhibitor concentration is shown in Fig. 5.

The value of corrosion rate was calculated from the following equation [25]:

$$k = \frac{\Delta W}{A.t} \quad (6)$$

Fcalculated using the following equations 7 and 8, respectively. [26, 27]:

$$\theta = \frac{k_o - k}{k_o} \quad (7)$$

$$\eta_w = \frac{k_o - k}{k_o} \times 100 \quad (8)$$

where k_o and k are the values of the corrosion rate without and with addition of the inhibitor, respectively.

Table.3. Corrosion parameters for steel in 1.0 M HCl in the absence and presence of different concentrations of PAAB at 30ºC.

Concentration (M)	Corrosion rate k ($mg.cm^{-2}.h^{-1}$)	η_w	θ
0 $x10^{-4}$	15.86 x 10^{-2}	---	---
1 $x10^{-4}$	7.27 x 10^{-2}	42.91	0.43
3 $x10^{-4}$	4.90 x 10^{-2}	69.11	0.69
5 $x10^{-4}$	2.62 x 10^{-2}	83.48	0.83
7 $x10^{-4}$	2.03 x 10^{-2}	87.18	0.87
9 $x10^{-4}$	1.53 x 10^{-2}	90.36	0.90

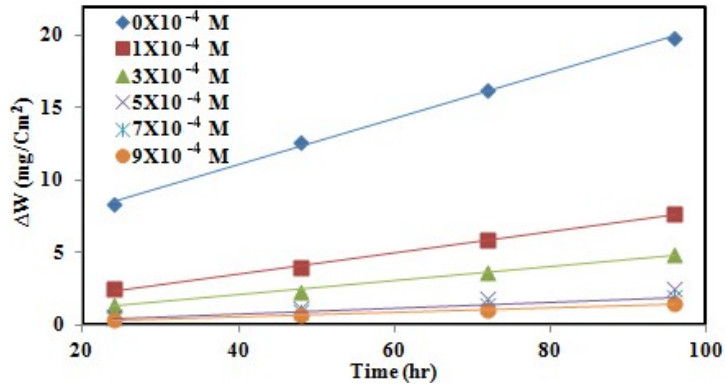

Fig.4. Variation of weight loss with exposure time for steel corrosion in 1.0 M HCl in the presence and absence of PAAB at 30 ºC.

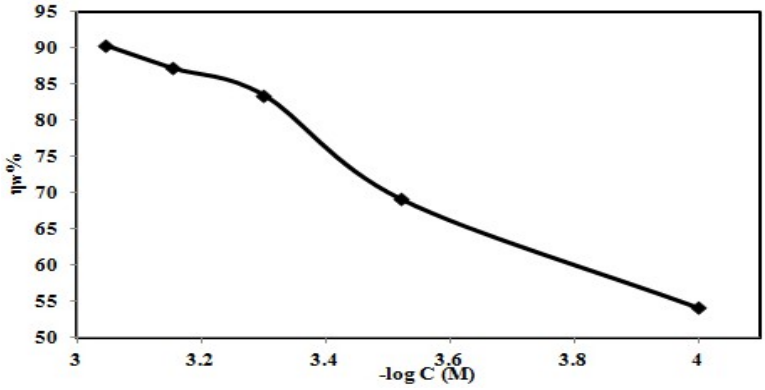

Fig. 5. Variation of the inhibition efficiency with concentration of the inhibitor at 30 ºC.

Adsorption consideration

It is well known that the adsorption of the inhibitor at the metal solution interface is the first step in the inhibition process. Depending on the type of interaction between inhibitor and metal solution interface, there are two types of adsorption on the electrode surface: physical adsorption and chemisorption. Physical adsorption comes from electrostatic attraction between electrically charged metal surface and charged species in the bulk of solution. Chemisorption is due to the charge transfer or charge sharing from the inhibitor molecules to the surface of metal and may be a back donation from metal to the inhibitor molecules. So, several adsorption isotherms were tested for the description of adsorption behavior of the studied

compounds and it was found that the adsorption of the studied PAAB on the steel surface in HCl solution obeys the Langmuir adsorption isotherm which expressed as:

$$\frac{\theta}{1-\theta} = KC \tag{9}$$

Or

$$\frac{C}{\theta} = \frac{1}{K} + C \tag{10}$$

where K is the equilibrium constant of the adsorption process and C the inhibitor concentration.

The best fitted straight line was obtained from the plot of C/θ against C, Fig. 6. The correlation coefficient (R^2) was used to choose the isotherm that best fit with the experimental data Table 4.

It is known that K_{ads} denotes to the strength between adsorbate and adsorbent. Large values of K_{ads} imply more adsorption and hence better inhibition efficiency [28]. The results showed high value of K_{ads} indicating a strong interaction and a strong adsorption. So, chemical adsorption was probably occurred due to the charge transfer or charge sharing between PAAB and steel surface.

The relation between equilibrium constant of adsorption K_{ads} and the standard free energy ΔG^{o}_{ads} was given by the following equation:

$$K = \frac{1}{55.5} \exp\left(\frac{-\Delta G^{o}_{ads}}{RT}\right) \tag{11}$$

where R is the molar gas constant, T is the absolute temperature and 55.5 is the concentration of water expressed in molar. We can rearrange this equation to the following form:

$$\log K = -1.744 - \left(\frac{\Delta G^{o}_{ads}}{2.303\ RT}\right) \tag{12}$$

We can calculate the standard free energy from this equation. The negative values of ΔG^{o}_{ads} indicate the spontaneity of the adsorption process and stability of adsorbed layer on metal surface. High value of ΔG^{o}_{ads} indicates the chemical interaction between the adsorbed layer and metal surface which was considered as chemisorption. Generally, the values of ΔG_{ads} up to -20 $kJmol^{-1}$ were considered as physical adsorption while chemisorption is around -40 $kJmol^{-1}$ as a result of sharing

or transfer of electrons from inhibitor to the metal surface to form a coordinate type of bond [29].

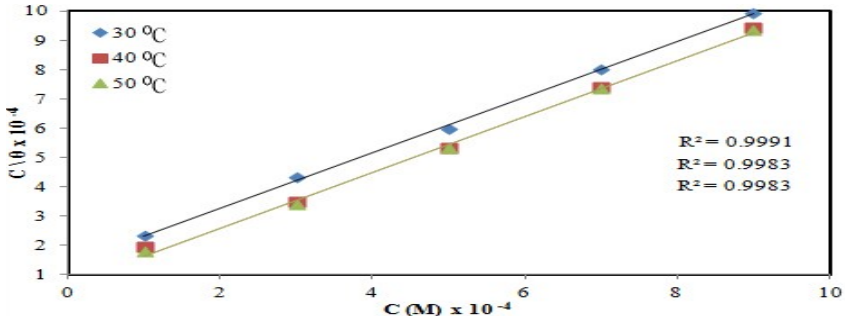

Fig.6. Langmuir adsorption plots for carbon steel in 1.0 M HCl at the presence of different concentrations of the inhibitor at different hhhhhtemperatures.

The adsorption heat was calculated according to the Van't Hoff equation [30]:

$$\ln K_{ads} = -\left(\frac{\Delta H^{o}_{ads}}{RT}\right) + const \qquad (13)$$

Where ΔH_{ads} and K_{ads} are the heat of adsorption and adsorptive equilibrium constant, respectively. It should be noted that $\Delta H_{ads} / R$ is the slope of the straight line $\ln K_{ads}$ against 1/T according to Eq. (13) and the molecular weight of inhibitor is also a positive constant, so the value of adsorption heat does not change with the unit of adsorptive equilibrium constant. The straight line $\ln K_{ads}$ against 1/T is shown in Fig. 7. ΔH^{o}_{ads} values are listed in Table 4. The positive values of ΔH_{ads} shows that the adsorption of the inhibitor is an endothermic process [31], which indicates that, the inhibition efficiency increases with increasing temperature. Such behavior can be interpreted on the basis that the increase in temperature resulted in adsorption of inhibitor molecules on the metal surface. The entropy of adsorption ΔS^{o}_{ads} was obtained using the basic thermodynamic equation:

$$\Delta G^{o}_{ads} = \Delta H^{o}_{ads} - T\,\Delta S^{o}_{ads} \qquad (14)$$

The values of ΔS_{ads} listed in Table 4 have a positive sign, as was expected, since the endothermic adsorption process is always accompanied by an increase of entropy. This increase of entropy was the driving force of the adsorption of inhibitor onto carbon steel surface [32, 33].

Table 4. Thermodynamic parameters using Langmuir adsorption isotherm on steel surface in 1.0 M HCl containing different vhhhhhh concentrations of PAAB at different temperature

Temp ^{o}k	K_{ads} (M^{-1})	ΔG_{ads} (KJ/mol)	ΔS_{ads} (J/mol .^{o}k)	ΔH_{ads} (KJ/mol)
303	7.178	-32.48	203.8	29.28
313	12.132	-33.81	201.5	29.28

323	14.695	-34.29	196.8	29.28

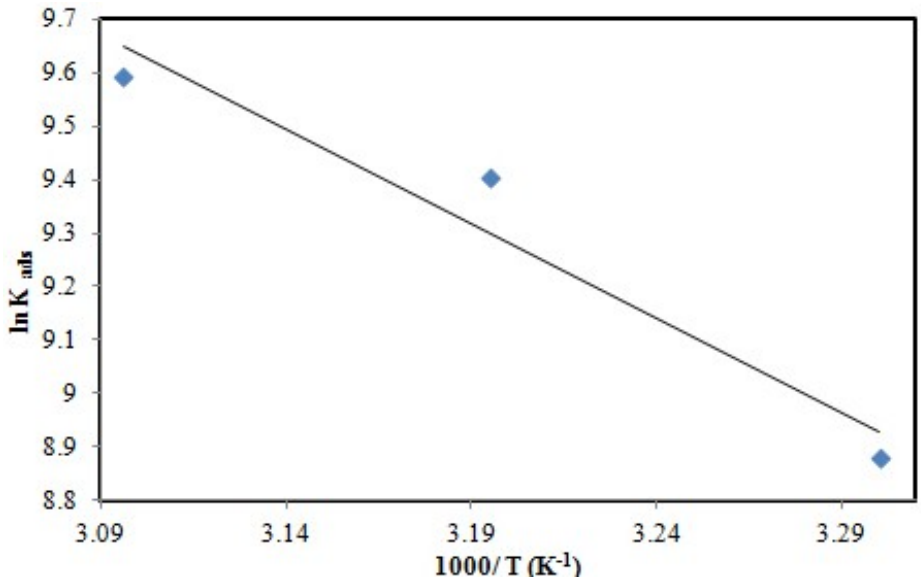

Fig.7. The plot of ln K_{ads} against 1/T.

Effect of temperatures

The corrosion rate of steel in 1.0 M HCl solution in the presence and absence of PAAB was studied at different temperatures (30, 40 and 50ºC) by weight loss measurements. The data in Table 5 shows that the inhibition efficiency (η_w) and surface coverage (θ) increased as the temperatures increased. These results are also shown in Fig.8.

Table 5. Weight loss data for carbon steel 1.0 M HCl without and with different concentrations of the synthesized surfactant at various temperatures

Conc.(M) $X10^{-4}$	40 ºC			50 ºC		
	$K(mg.cm^{-2}.h^{-1})$ $X\ 10^{-2}$	θ	η_w (%)	$K(mg.cm^{-2}.h^{-1})$ $X\ 10^{-2}$	θ	η_w (%)
0	66.29	--	--	76.25	--	--
1	32.68	0.50	50.70	33.58	0.55	55.96
3	9.54	0.85	85.61	9.38	0.87	87.69
5	4.07	0.93	93.85	4.57	0.93	93.99
7	3.697	0.94	94.42	3.63	0.95	95.22
9	3.01	0.95	95.46	2.88	0.96	96.21

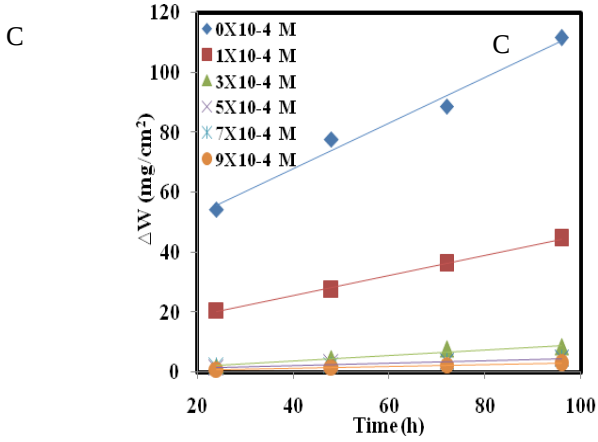

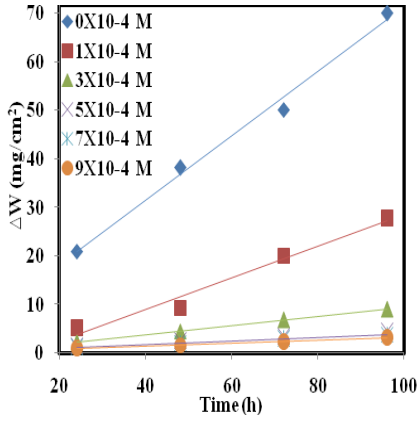

Fig. 8. Weight loss values at two different temperatures. (40, 50 ºC)

In acid medium, the corrosion rate is related to temperature by Arrhenius equation:

$$\log k = \log A - \frac{E_a}{2.303\ RT} \qquad (15)$$

where k is the corrosion rate determined from weight loss measurements, E_a is the apparent activation energy, A is the Arrhenius constant, R the molar gas constant and T is the absolute temperature. The apparent activation energy was determined from the slopes of log k against 1/T as shown in Fig. 9.

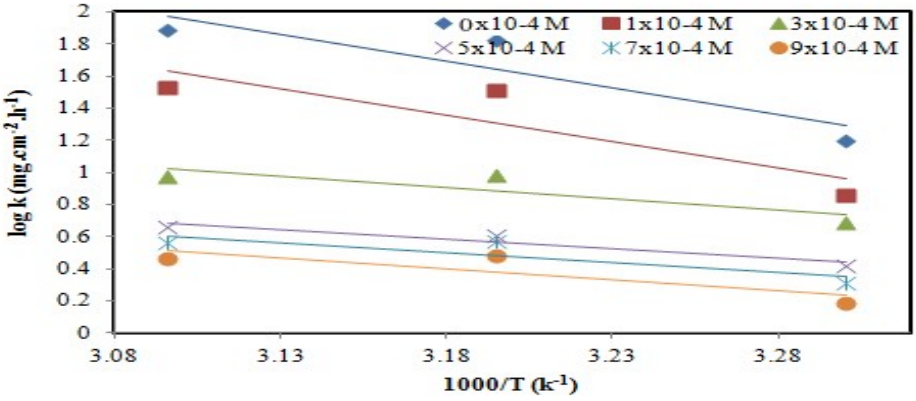

Fig. 9. Arrhenius plots (ln k versus 1/T) for carbon steel in 1.0 M HCl solution without and with different concentrations of the sdfghjinhibitor.

The values of enthalpy of activation ΔH* and entropy of activation ΔS* were obtained from the transition state equation

$$k = \left(\frac{RT}{Nh}\right) \exp\left(\frac{\Delta S^*}{R}\right) \exp\left(\frac{-\Delta H^*}{RT}\right) \qquad (16)$$

where h is Planck's constant and N is Avogadro's number.

A plot of log (k/T) as a function of 1/T Fig. 10 showed a straight line. ΔH* and ΔS* are calculated from the slope and intercept, respectively. The calculated values of the thermodynamic parameters of activation for the dissolution of steel at different temperatures are presented in Table 6. These data show that the values of both ΔH* and ΔS* in the presence of PAAB increase over that of blank which means that the energy barrier of corrosion reaction in the presence of PAAB increases. The positive values of ΔH* showed that the dissolution process is endothermic. The

decrease of value of ΔS* means that the decrease in disorder is due to the molecules oriented on the surface and ordered by adsorption through the active centers.

Table 6. Activation parameters values for steel in 1.0 M HCl in the absence and presence of different concentrations of the inhibitor

Conc. (M)	E_a (kJ mol^{-1})	ΔH* (kJ mol^{-1})	ΔS* (J mol^{-1} K^{-1})
0 x 10^{-4}	64.43	76.69	202.65
1 x 10^{-4}	62.88	77.42	196.13
3 x 10^{-4}	26.70	30.19	34.06
5 x 10^{-4}	22.77	27.15	15.89
7 x 10^{-4}	23.90	29.60	21.51
9 x 10^{-4}	26.04	33.49	31.17

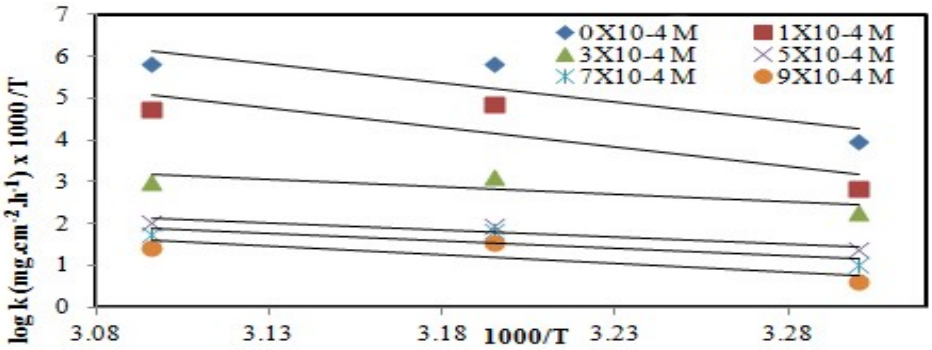

Fig.10. Arrhenius plots of the corrosion rate for carbon steel in 1.0 M HCl in absence and presence of inhibitor at 30, 40 and 50 ◦C.

Polarization Measurements:

Fig.11. shows representative anodic and cathodic polarization curves of steel in 1.0 M HCl solutions in the absence and presence of various concentrations of the inhibitor. In the presence of inhibitor at high concentrations (7×10^{-4} and 9×10^{-4}M), the E_{corr} values are slightly shifted toward the negative direction in comparison to the results obtained in the absence of the inhibitor. Both the anodic and cathodic current densities are decreased by the inhibitor, but the cathodic curves are affected to a greater extent. This result suggests that the inhibitor suppressed both the anodic and cathodic reactions, although mainly the cathodic one [34]. While at low concentrations (1×10^{-4}, 3×10^{-4}, and 5×10^{-4}M), the E_{corr} values are slightly shifted toward the positive direction in comparison to the results obtained in the absence of the inhibitor and the anodic inhibiting effect becomes more significant. These findings suggest that the inhibiting action of the inhibitor and the adsorption mode on metal surface highly influenced by the concentration of the inhibitor. This may be due to that at low concentrations of the inhibitor (surfactant) can be adsorbed completely on metal surface by both hydrophobic and hydrophilic parts while at high concentrations the adsorption takes place only by the hydrophobic part on surface.

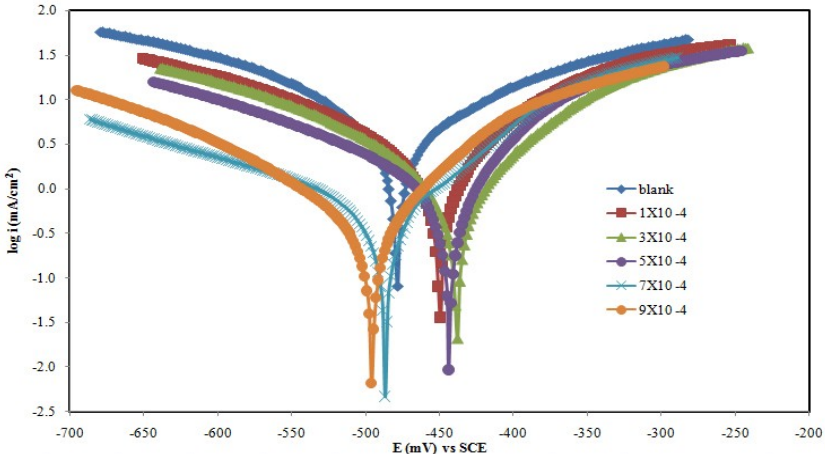

Fig.11. Tafel polarization curves of steel in 1.0 M HCl solutions containing various concentrations of inhibitor.

The electrochemical parameters such as corrosion potential (E_{corr}), corrosion current density (i_{corr}), cathodic Tafel slope (βc), and anodic Tafel slope (βa) obtained from the polarization curves and the corresponding inhibition efficiency (η_p) values at different inhibitor concentrations are reported in **Table 7.**

Table 7. Electrochemical parameters for steel in 1.0 M HCl solution containing different concentrations of the inhibitor

Conc.	E_{corr} vs.SCE(mV)	I_{corr} (mA cm^{-2})	β_a (mV dec^{-1})	β_c (mV dec^{-1})	Rp ($\Omega.cm^2$)	C.R (mm y^{-1})	θ	η_p%
0×10^{-4}	-478.4	8.2353	250.6	-218.3	5.73	96.32	-----	----
1×10^{-4}	-449.6	4.3571	162.8	-244.5	12.89	50.96	0.47	47.09
3×10^{-4}	-438.2	2.5122	138.1	-203.4	21.40	29.38	0.69	69.49
5×10^{-4}	-443.5	1.9485	108.0	-219.6	21.42	22.79	0.76	76.33
7×10^{-4}	-486.6	0.6324	92.6	-205.1	38.74	7.396	0.92	92.32
9×10^{-4}	-495.7	0.4534	79.2	-120.5	45.11	5.302	0.94	94.49

Inspection of the η_p values revealed that inhibition efficiency increases with increasing concentration of inhibitor (Table 7 and Fig .11.). It can be observed that the values of corrosion current density (i_{corr}) of steel in the presence of the inhibitor were lower than those for the inhibitor-free solution. This suggests that the compound was adsorbed on the metal surface and retarding the corrosion reaction. The increase in inhibition efficiency observed at higher inhibitor concentrations indicates that more inhibitor molecules were adsorbed on the metal surface, thus providing wider surface coverage and that this compound acted as adsorption inhibitor.

Scanning electron microscopy (SEM)

Immersion corrosion analysis of steel samples in the acidic solutions with and without the inhibitor was performed using SEM. After 24 hours immersion in 1.0 M HCl, the samples were subjected to SEM studies to know the surface morphology. SEM Jeol JSM-5400 was used for the experiments. The SEM micrographs of the corroded steel in the presence of 1.0 M HCl solution is shown in Fig. 12a. The faceting seen in this figure was a result of pits formed due to the exposure of steel to the acid. The influence of the inhibitor addition (9×10^{-4} M) on the steel in 1.0 M HCl solution is shown in Fig. 12b. The faceting observed in figures disappeared and the surface was free from pits and it was smooth. It can be concluded that corrosion does not occur in presence of inhibitor and hence corrosion was inhibited strongly when the inhibitor was present in the hydrochloric acid.

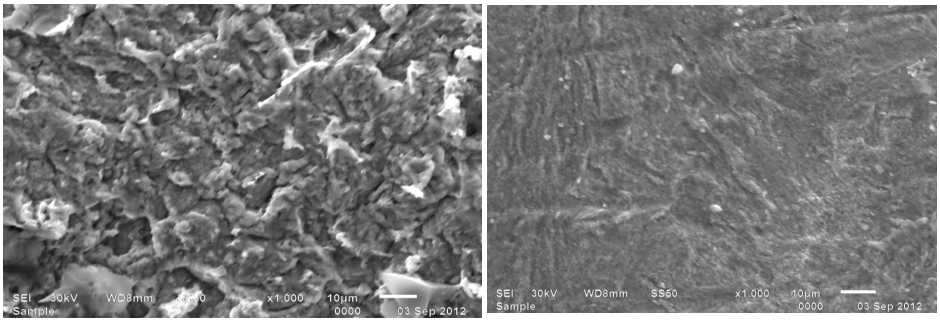

Fig. 12. SEM image of surface of carbon steel after immersion for 24 h in 1.0 M HCl at

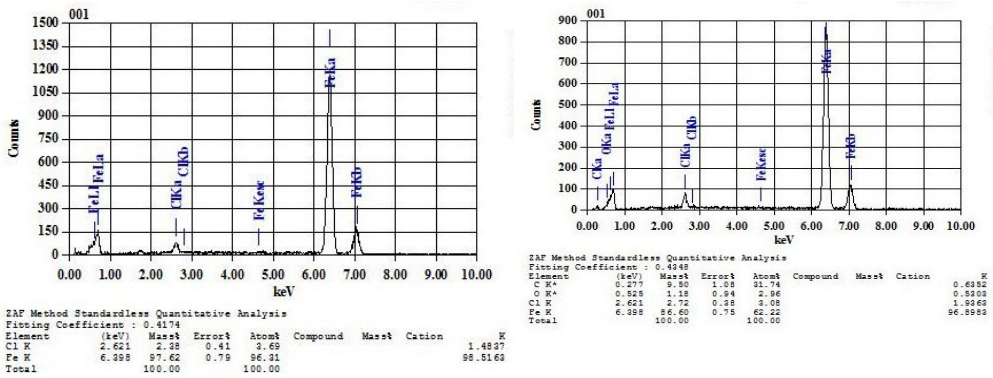

Fig. 13. EDX spectra recorded for steel specimens immersed in 1.0 M HCl for 24 h in the absence and presence of $9x10^{-4}$ M of the inhibitor at 25 °C.

Quantum chemical calculations

Quantum chemical calculations were performed to investigate the effect of structural parameters on the inhibition efficiency of the inhibitor and study its adsorption mechanism on the metal surface. The calculations were done using semi empirical method (PM6). Geometric and electronic structure of the inhibitor was calculated by the optimization of his bond length, bond angle and dihedral angle. The optimized structure and bond lengths are shown in Fig.14.

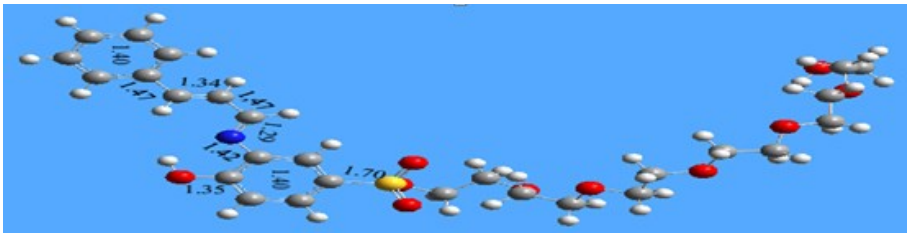

Fig.14 .The optimized molecular structure and bond length for the investigated compound.

It was shown from the calculations of geometrical structure of the investigated compounds that the bond lengths within the ring moiety approximately 1.40 Å (conjugated system), 1.34 Å (sp^2 hyperdization) for C=C and 1.47Å (sp^3 hyperdization) for C-C. The N=C bond has the shortest bond length1.29 Å (formation of a double bond, sp2 hybridization.) while C-S bond has the longest bond length 1.70 Å. For the substituted hydroxyl group on ring, the bond length 1.35Å. The results also showed that the two rings not in the same plane but perpendicular to each other.

Quantum chemical parameters obtained from the calculations which are responsible for the inhibition efficiency of inhibitors, such as the energies of highest occupied molecular orbital (E_{HOMO}), energy of lowest unoccupied molecular orbital (E_{LUMO}), the separation energy (E_{LUMO} - E_{HOMO}), ΔE, representing the function of reactivity, dipole moment, μ, summation of the total negative charges on atoms over the skeleton of the molecule (TNC), total energy (TE), and molecular volumes of molecule (MV), are collected in Table8,

Table 8. Quantum chemical parameters of the investigated inhibitor

E_{HOMO} (ev)	E_{LUMO} (ev)	ΔE (ev)	μ (D)	TNC (e)	TE (ev)	MV (cm^3/mol)
-9.31	-1.23	8.08	4.91	-8.90	14.68	652.63

The inhibition effect of the inhibitor usually depends on the adsorption of those molecules on the metal surface. The adsorption on the metal surface could happen through three modes according to the molecular structures. The first is as neutral molecule via chemisorption mechanism involved sharing of lone pairs of electrons between electronegative atoms and metal. The second is through the intermolecular force, which is relevant to the dipole of the inhibitors. The third is through the plane conjugating system of the aromatic ring, which donate π electrons to the metal surface, accept electrons from metal surface and the intercalation of hyperconjucating system. The calculations showed that there is more than one active center by which the inhibitor would be adsorbed on the metal surface. The expected adsorption mechanism for the inhibitor on the metal surface is mixed type mechanism; physical adsorption resulting from the intermolecular force between the charged centers of molecules and the metal surface, as the calculated Mulliken charges show that there are more than one active center (-ph-**O**H = -0.429,-C=**N**- = -0.321, -S=**O** = -0.923, and -S-**O**H = -0.720) and it was confirmed that the more negative the atomic partial charges of the adsorbed center are, the more easily the atoms donate its electrons to the unoccupied d-orbital of the metal [35]. Chemical

adsorption also resulting from the donation of π-electrons of benzene ring moiety and the lone pair of electrons from N atom to the metal. To understand the adsorption more the interaction of the inhibitor compound with one Fe atom simply reveals three single bonds formation (Fe-N, Fe-O-ph and Fe-C) coincides with that found for the distance of chemisorption of inhibitor with metal [36-38], forming two new stable five membered rings as shown in Fig.14.

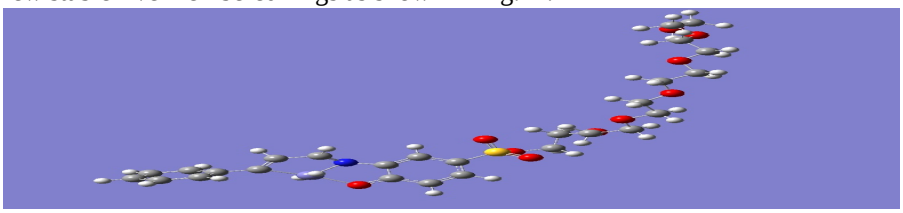

Fig.14. The optimized structure of Fe-Inhibitor

Molecular dynamic simulations

Molecular dynamics were performed on a system comprising a PAAB molecules and steel surface. PAAB molecules were optimized first and then run quench molecular dynamics. Fig.15. shows the optimization energy curves for the PAAB molecules, before placing them on the iron surface.

Adsorption calculations were done on PAAB/iron to find the lowest energy for the whole system. The outputs and descriptors are presented in Table 9 included the total energy, in kcal mol^{-1}, of the substrate–adsorbate configuration. The total energy is defined as the sum of the energies of the adsorbate components (the rigid adsorption energy and the deformation energy). In this study, adsorption energy, in kcal mol^{-1}, reports energy released (or required) when the relaxed adsorbate components are adsorbed on the substrate. Table 9 shows also ($dE_{ads/dNi}$), which reports the energy, in kcal mol^{-1}, of substrate–adsorbate configurations where one of the adsorbate components has been removed . High values of adsorption energy indicate that the molecule will give the highest inhibition efficiency. The shape of PAAB molecules on metal surface is shown in Fig.16.

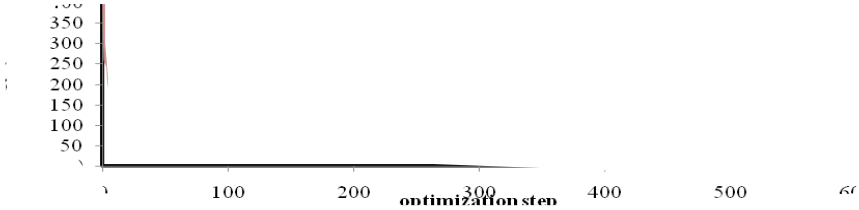

Fig .15.Optimization energy curves for inhibitor before placing on surface of metal.

Table 9. The calculated descriptors obtained from molecular dynamics calculations.

Total energy	Adsorption energy	Rigid adsorption energy	Deformation energy	dEads/dNi
-341.57	-853.36	-332.56	-520.80	-853.36

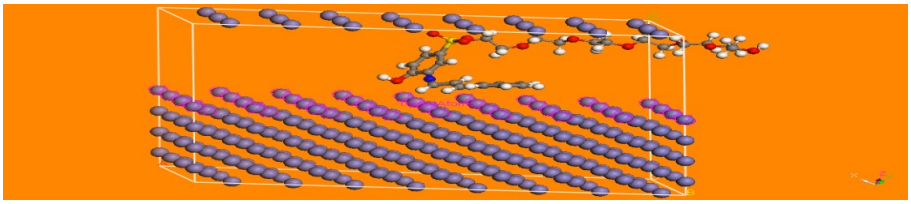

Fig.16. Molecular simulations for the most favorable modes of adsorption obtained for the investigated inhibitors on Fe (1 1 1) smmmsurface.

References:

1. J. Aljourani, K. Raeissi and M.A. Golozar, Corros. Sci., **51** (2009) 1836–1843.
2. K.C. Emregul and O. Atakol, Mater. Chem. Phys. **82** (2003) 188–193.
3. A. Asan, M. Kabasakalog˘lu, M. Is kalan and Z. Kılıc, Corros., Sci. **47** (2005) 1534–1544.
4. K. Stanly Jacob and G. Parameswaran, Corros., Sci. **52** (2010) 224–228.
5. Y. Tang, X. Yang, W. Yang and Y. Chen, R. Wana, Corros., Sci. **52** (2010) 242–249.
6. P. Lowmunkhong, D. Ungthararak and P. Sutthivaiyakit, Corros., Sci. **52** (2010) 30–36.
7. M. Abdallah, Corros. Sci., **44** (2002) 717–728.
8. M.A. Hegazy, Corros. Sci., **51** (2009) 2610–2618.
9. R. Hasanov, S. Bilge, S. Bilgic, G. Gece and Z. Kılıc, Corros. Sci., **52** (2010) 984–990.
10. A. Chetouani, A. Aouniti, B. Hammouti, N. Benchat, T. Benhadda and S. Kertit, Corros. Sci., **45** (2003) 1675–1684.
11. A. Lgamri, H. Abou El-Makarim, A. Guebour, A. Ben Bachir, L. Aries and S. El Hajjaji, Prog. Org. Coat., **48** (2003) 63–70.
12. Y.K. Agrawal, J.D. Talati, M.D. Shah, M.N. Desai and N.K. Shah, Corros. Sci., **46** (2004) 633.
13. D.N. Singh and A.K. Dey, Corrosion., **49** (1993) 594.
14. G. Banerjee and S.N. Malhotra, Corrosion., **48** (1992) 10.
15. S.T. Arab, E.A. Noor, Corrosion **49** (1993) 122.
16. L.A. Raspi, Nickel Corros., **49** (1993) 821.
17. Y. Chen, Y. Wang and G. Zhang, Daily Chem., Ind. **2** (1986) 56.
18. L. Shi, H. Song, Daily Chem. Ind. **1** (1987) 9.

19. Gaussian 09, Revision A.02, M. J. Frisch, G. W. Trucks, H. B. Schlegel, G. E. Scuseria, M. A. Robb, J. R. Cheeseman, G. Scalmani, V. Barone, B. Mennucci, G. A. Petersson, H. Nakatsuji, M. Caricato, X. Li, H. P. Hratchian, A. F. Izmaylov, J. Bloino, G. Zheng, J. L. Sonnenberg, M. Hada, M. Ehara, K. Toyota, R. Fukuda, J. Hasegawa, M. Ishida, T. Nakajima, Y. Honda, O. Kitao, H. Nakai, T. Vreven, J. A. Montgomery, Jr., J. E. Peralta, F. Ogliaro, M. Bearpark, J. J. Heyd, E. Brothers, K. N. Kudin, V. N. Staroverov, R. Kobayashi, J. Normand, K. Raghavachari, A. Rendell, J. C. Burant, S. S. Iyengar, J. Tomasi, M. Cossi, N. Rega, J. M. Millam, M. Klene, J. E. Knox, J. B. Cross, V. Bakken, C. Adamo, J. Jaramillo, R. Gomperts, R. E. Stratmann, O. Yazyev, A. J. Austin, R. Cammi, C. Pomelli, J. W. Ochterski, R. L. Martin, K. Morokuma, V. G. Zakrzewski, G. A. Voth, P. Salvador, J. J. Dannenberg, S. Dapprich, A. D. Daniels, O. Farkas, J. B. Foresman, J. V. Ortiz, J. Cioslowski, and D. J. Fox, Gaussian, Inc., Wallingford CT, 2009.

20. V.S. Sastri and J.R. Perumareddi, Corrosion., **53** (1996) 671.

21. R.G. Pearson, Inorg. Chem., **27** (1988) 734.

22. S. Martinez, Mater. Chem. Phys., **77** (2002) 97.

23. J. Barriga, B. Coto and B. Fernandez, Tribol., Int. **40** (2007) 960.

24. H. Sun, P. Ren and J.R. Fried, Comput. Theor. Polym., Sci. **8** (1998) 229.

25. L.B. Tang, G.N. Mu and G.H. Liu, Corros. Sci. **45** (2003) 2251.

26. P. Manjula, S. Manonmani, P. Jayaram and S. Rajendran, Anti-Corros., Methods Mater. **48** (2001) 319.

27. S.S. Abdel-Rehim, A.M. Magdy and K.F. Khaled, Mater. Chem. Phys., **70** (2001) 268.

28. L. Tang, X. Li, Y. Si, G. Mu and G.H. Liu, Mater., Chem. Phys. **95** (2006) 26.

29. S.A. Umoren, I.B. Obot and E.E. Ebenso, E.J. Chem. **5** (2008) 355.

30. G. Quartarone, M. Battilana, L. Bonaldo and T. Tortato, Corros., Sci. **50** (2008) 3467–3474.

31. M.A. Hegazy, H.M. Ahmed and A.S. El-Tabei, Corros., Sci. **53** (2011) 671–678.

32. L. Finar, Organic chemistry, 6th Ed., Vol. 1, Longman, 1986.

33. G.N. Mu, X.H. Li and Q. Qu, J. Zhou, Acta Chim. Sinica., **62** (2004) 2386–2394.

34. A. A. El-Sayed, Corros. Prev. Control., **43** (1996) 23–27.

35. K.F. Khaled, J. Electrochimica Acta., **53** (2008) 3484.

36. D. Curulla-Ferre, A. Govender, T. C. Bromfield and J. W. Niemantsverdriet. *J. Phys. Chem., B* **110** *(*2006) 13897.

37. D.E. Jiang and B. G. Sumpter, S.Dai, *J. Am. Chem. Soc*., **128** *(*2006) 6030.

38. C. Combellas, M. Delamar, F.J. Kanoufi, Pinson and F. I .Podvorica,. *Chem. Mater.*, **17** *(*2005) 3968.

[1]HNMR spectrum

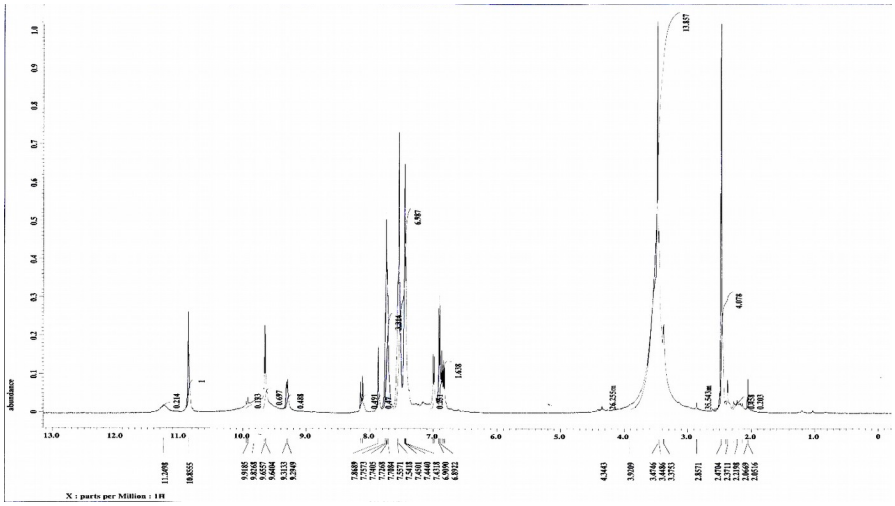

[1]HNMR (DMSO) spectrum (Fig.2) showed different bands at δ=10.8555 ppm (s, 1H, (phenolic)–O**H**; δ=9.6557 ppm (s, 1H, N=C**H**); δ=7.7573-7.8689 ppm (d, 2H, m-phenolic nucleus); δ=7.7084–7.7573 ppm (d, 2H, o-benzelidine nucleus); δ=7.4501–7.5571 ppm (t, 3H, m,p-benzelidine nucleus); δ=6.8922 ppm (t, 1H, ph-CH=CH);δ=6.9090 ppm (d, 1H, ph-CH=CH); δ=3.3753-3.4746 ppm (t, 20H, $OSO(OCH_2CH_2)_n$); and δ=2.3711-2.4704ppm (t, 2H, OCH_2CH_2OH). The data of [1]HNMR spectra confirmed the expected hydrogen proton distribution in the synthesized inhibitor.

Mass spectrum

The mass spectrum (Fig. 3) of the synthesized inhibitor illustrated a molecular ion peak at m/z586 (73.11%) together with other significant peaks, which were observed at m/z (intensity %): base peak at 85 (100 % HN=CHCH=$CHCH_2OH$), 56 (34.45 % HN=CHCH=CH_2), 117 (68.07 % CH_2CH=CH-ph), 121 (52.94 % HO-ph-N=CH_2), 130 (46.22 % N=CHCH=CH-ph), 133 (17.65 % HO-ph-N=$CHCH_2$), 146 (52.94 % HO-ph-N=CHCH=CH_2), 207 (68.91 % ph-N=CHCH=CH-ph), 221 (46.22 % O-ph-N=CHCH=CH-ph). Data of mass spectrum confirmed the chemical structure of the synthesized Schiff base surfactant.

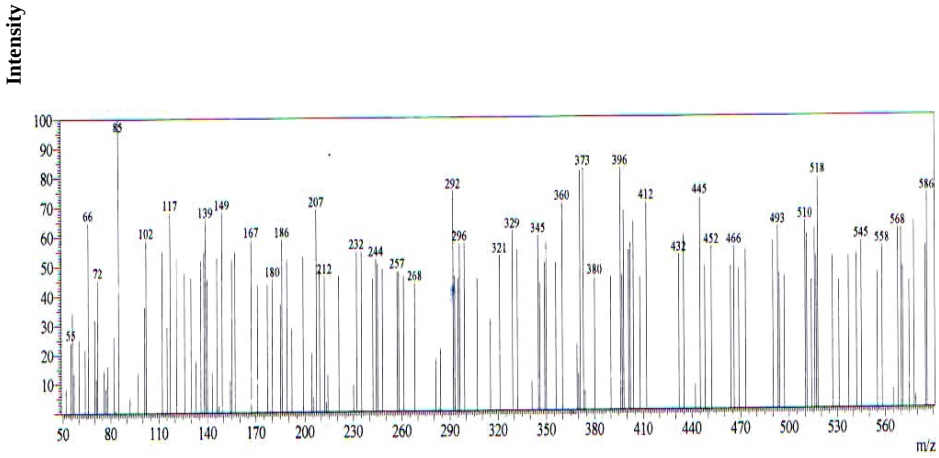

Fig.3. Mass spectrum of the synthesized Schiff base surfactant

C, H, N and S elemental analysis

C, H, N and S elemental analysis (Table 2) showed that the elemental percent of the theoretical and experimental data are closed approximately. This indicates that the synthesized inhibitor is very pure.

Table.2. C, H, N and S elemental analysis of the synthesized Schiff base surfactant

Element %